Resonance Raman scattering from phonon overtones in double-wall carbon nanotubes

R. Pfeiffer,[1] H. Kuzmany,[1] F. Simon,[1] S. N. Bokova,[2] and E. Obraztsova[2]
[1]*Universität Wien, Institut für Materialphysik, Strudlhofgasse 4, A-1090 Wien, Austria*
[2]*Natural Sciences Center of A. M. Prokhorov General Physics Institute of Russian Academy of Sciences, 38 Vavilov Street, 119991 Moscow, Russia*

(Received 13 September 2004; revised manuscript received 22 December 2004; published 15 April 2005)

The resonance behavior and the dispersion of the G′ line in double-wall carbon nanotubes were investigated by multifrequency Raman scattering. Using a large number of laser lines for excitation, the dispersion for the response from the inner tubes and from the outer tubes was found to be 85 and 99 cm^{-1}/eV, respectively. The reduction of the dispersion for the inner tubes is a consequence of their high curvature and suggests a flattening of the phonon dispersion at the *K* point in the Brillouin zone. The frequency position for the G′ line of the inner tubes for a given laser energy was likewise strongly reduced as compared to values expected from tubes with standard diameter. This was again assigned to the strong curvature of the small-diameter inner tubes. Finally, the G′ line scattering cross sections for the outer tubes and for the inner tubes revealed resonances according to the transitions between the corresponding Van Hove singularities. The response from the inner tubes was particularly strong, in good agreement with the expected resonance enhancement resulting from their high curvature.

DOI: 10.1103/PhysRevB.71.155409 PACS number(s): 78.67.Ch, 61.46.+w, 78.30.Na, 63.20.Dj

I. INTRODUCTION

Single-wall carbon nanotubes (SWCNTs) have been attracting considerable interest for a number of years as they are very good examples for one-dimensional systems on the one hand and exhibit a high application potential on the other hand.[1–3] Recently, particular attention has been dedicated to double-wall carbon nanotubes (DWCNTs). Such systems are of special interest if the inner shell tubes are grown from fullerenes encapsulated into the primary outer shell tubes (so-called peapods[4]).[5] On heating to temperatures as high as 1250 °C, the fullerenes in the peapods transform into inner shell tubes with a high degree of perfectness.[6]

Peapod grown DWCNTs are exceptional for several reasons. Normally, peapods are obtained from SWCNTs with mean tube diameters between 1.3 and 1.5 nm. Since the intertube distance in the DWCNTs is about 0.35 nm (the interlayer distance in graphite), the diameters of the inner shell tubes are around 0.7 nm, coming close to SWCNTs grown in zeolites.[7,8] The diameter distribution of the inner tubes is expected to follow roughly the distribution of the outer ones, except for a cutoff below 0.5 nm.[9] This cutoff is a consequence of the rather large size of the fullerenes which cannot enter tubes with diameters smaller than about 1.2 nm.

Referring to applications, DWCNTs share the advantages of multiwall tubes in a sense that they are rather stiff and properties from the two shells average out. Conversely, they still have some advantages of SWCNTs, e.g., small diameters and low weight. For fundamental research, the very small radii of the inner tubes are of particular interest. Additionally, the unit cells become small enough to allow for application of density-functional calculations. Such calculations are indeed necessary to describe the physical properties as a consequence of the high curvature of the narrow tubes.

One of the famous and important properties of the SWCNTs is their electronic structure. Due to the one-dimensional nature of the tubes, the electronic density of states is jammed into Van Hove singularities (VHSs). Within a simple tight-binding approximation, optical transitions are between VHSs symmetric to the Fermi level. The transition energies for semiconducting and metallic tubes are assigned as E_{ii}^{S} and E_{ii}^{M}, respectively. In a linear approximation, these energies scale with $1/D$, where D is the tube diameter.[10] In a refined description, the trigonal warping of constant energy contours and the influence of the chirality must be considered.[10] Symmetry-adapted nonorthogonal tight-binding calculations yield more precise results with lower transition energies and a stronger deviation from a $1/D$ law since tube curvature is included.[11] In addition, the exact values for the electronic energies are modulated by excitonic effects, particularly for the low i transitions[12] and by the effect of bundling or dressing with surfactants. Finally, and certainly of particular importance for very small inner shell tubes, the influence of the curvature must be considered explicitly. If the tube diameters become significantly lower than 1 nm, characteristic differences in the electronic structure as compared to tight-binding results were reported from *ab initio* calculations.[13]

A plot of the transition energies versus tube diameter for all geometrically allowed tubes, known as the Kataura plot,[14] is very helpful and important to understand optical and resonance Raman effects. The plot depicted in Fig. 1, with the inverse tube diameter used on the abscissa, is based on calculations by Popov.[11] The calculated energies from this work were subsequently scaled to match the experimental ones of Fantini *et al.*[15] and Weisman and Bachilo[16] (obtained from HiPco tubes dispersed in aqueous solution and wrapped in SDS). The scaling factors for each transition and SWCNT type (metallic as well as semiconducting type I and II) depended linearly on the inverse tube diameter. The horizontally hatched area marks the range of laser energies used in our experiments. The vertically hatched areas mark the diameter distribution of the outer (left) and inner tubes (right), respectively.

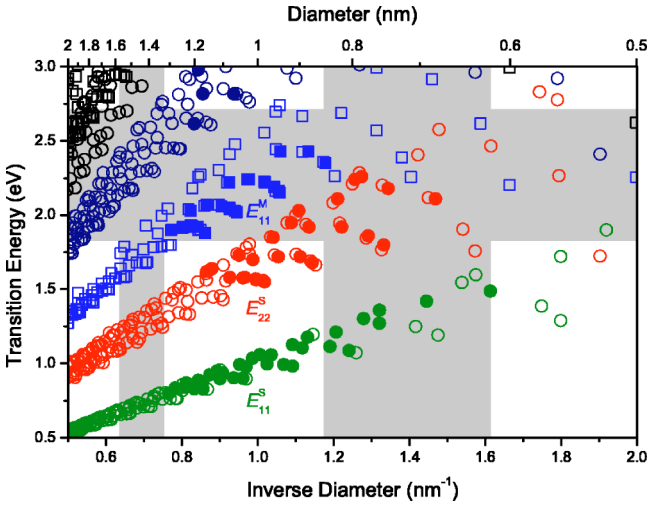

FIG. 1. Transition energies vs inverse diameter of SWCNTs (Kataura plot), based on calculations by Popov (Ref. 11) (open symbols). The calculated energies were scaled to fit the experimental results of Fantini *et al.* (Ref. 15) (filled symbols for E_{22}^{S} and E_{11}^{M}). The E_{11}^{S} branch was taken from Weisman and Bachilo (Ref. 16). The hatched areas assign the energy range used for excitation of Raman spectra (horizontally) and the tube diameter ranges for outer (left) and inner tubes (right). The widths of the vertical bars are the FWHMs of the assumed Gaussian distributions.

Raman spectroscopy has been demonstrated in numerous experiments to be a key analytical technique for the investigation of SWCNTs. The resonance enhancement for transitions between VHSs makes the technique particularly appealing. Four characteristic Raman modes are known: The radial breathing mode (RBM) around 180 cm^{-1}, the defect line (D mode) around 1350 cm^{-1}, the graphitic mode around 1590 cm^{-1} (G mode), and the overtone of the D mode around 2700 cm^{-1} (G′ or D* mode).

For all lines, the frequency depends on the tube diameter. This dependence is rather strong and scales as the inverse tube diameter for the RBM whose frequency increases with decreasing diameter.[17,18] The frequencies for the other Raman lines also depend on the inverse diameter, however they decrease with decreasing tube diameter.[19,20]

Additionally, the line position depends also on the energy of the exciting laser. This holds at least for the RBM, the D line, and the G′ line and is known as dispersion of the Raman modes. The origin of the dispersion is characteristically different for the RBM response on the one side and for the D and the G′ lines on the other side. In the former case, it is related to a photoselective resonance scattering which requires a distribution of tube diameters in the sample. In contrast, in the case of the D line and the G′ line, the response comes from phonons related to the *K* point in graphene, or from phonons close to this point.[21,22] A double resonance scattering process was found to be the origin of the dispersion,[22] similarly to what has been reported for graphene,[21] and the magnitude of the effect (shift in line position versus change in excitation energy) is determined by the slope of the phonon dispersion near the *K* point in graphite.[23]

Double resonance Raman scattering is well known in resonance Raman theory. It was recently applied to understand the D line in SWCNTs in a quantitative manner.[22–24] To satisfy energy and momentum conservation, scattering by an impurity must be included into the overall Raman process for the D line. For the double resonance leading to the G′ line, the process is similar but no contribution from a defect is required, rather a second phonon takes care for momentum conservation. The principle of this mechanism as it is operating for the two-phonon process is depicted in Fig. 2.

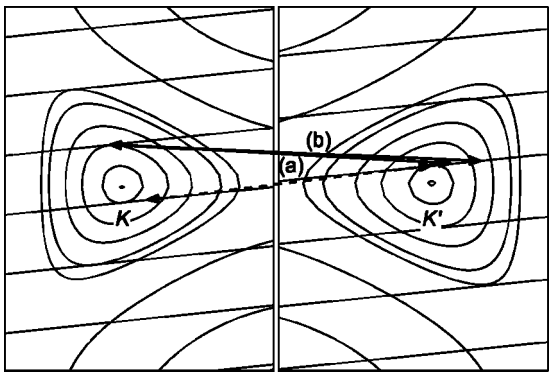

FIG. 2. Double resonance scattering for the Raman response of the G′ line in SWCNTs. Closed curves: equal energy contours of the graphene band structure, parallel lines: allowed *k* states for an (8, 4) tube. Full drawn arrows represent double resonance scattering processes for the incoming (a) and for the outgoing (b) light where Van Hove singularities are involved (triple resonance). The dashed arrow represents also a triple resonance but with less efficiency.

The figure depicts contours of equal energy at two neighboring *K* points of the graphene band structure. The parallel lines are the allowed *k* states for an (8, 4) tube. The two full drawn arrows depict two examples for particular strong resonance enhancements (triple resonance).[23] For the arrow (a) the primary electron-hole excitation meets a transition between two VHSs (ingoing resonance). The scattering from *K* to *K′* by the phonon $(\hbar\Omega_q, q)$ ends on an eigenstate of the tube which is in general not a VHS. Backscattering by the phonon $(\hbar\Omega_q, -q)$ takes the electron back to its original *k* value but at an energy $2\hbar\Omega_q$ below the eigenstate (for Stokes scattering). The final recombination is therefore nonresonant. For the outgoing resonance [vector (b)], the primary electron-hole excitation is nonresonant, scattering is to a SWCNT state on the *K′* position, and backscattering is into the VHS on the *K* position. As far as the incoming light is concerned, the difference in energy between the two resonances is as large as $2\hbar\Omega_q = 0.33$ eV, where *q* is (almost) the wave vector of the *K* point phonon. An alternative but less efficient triple resonance occurs if the electron is scattered to the VHS on the *K′* side and either the primary excitation or the final recombination is nonresonant. In all cases, two transitions are in resonance whereas the third transition is off resonance. In addition, for the triple resonance, of the ingoing and outgoing resonance, two VHSs are involved. Double resonance may as well occur between any two appropriate states on the two *K* points. It does not need the VHSs. This means the expected resonance profiles may be rather broad. The theory for double resonance scattering for the G′ line is more complicated than the theory for the D line, since the two-phonon density of states for the *K* point derived phonons

has to be considered. As a consequence of the zone folding, many branches can contribute.

Whereas considerable investigations have been dedicated to the RBM analysis in the DWCNTs,[6,25] very little has been reported on the G line response[26] and almost nothing is known about the D and G′ lines. The D line response is important since its intensity is related to the number of defects in the tubes. Since the RBM response from the inner shell tubes exhibits unusual narrow lines,[6] the relative concentration of the defects must be small and only a weak D line response is expected. On the other hand, small tube diameters enhance the electron-phonon (e-ph) coupling[27] which raises Raman intensities. Unfortunately, the D line of SWCNTs exhibits a structured profile[24] as a consequence of the resonance from the VHSs and the warped energy contours. Since the diameter dependence of the D mode frequency is rather small,[19] the contributions from inner and outer shell tubes overlap in general and are not easy to separate. Therefore, in this contribution we concentrate on the behavior of the G′ line where the separation between response from the inner tubes and outer tubes is twice as high as for the D line. Since the G′ line response is independent of any defect concentration and the inner tube response still gains from enhanced e-ph coupling, a strong signal from the inner tubes is expected.

The response from the outer and from the inner tubes was indeed found to be well separated. In fact, the separation was more than twice as strong as expected from results reported previously for the diameter dependence of this mode as analyzed from individual SWCNTs.[19] Peak resonances were different for the two-tube species but could be correlated to ingoing and outgoing resonances of the light with respect to VHSs. The resonance cross section was strongly enhanced for the inner shell tubes but explicit evaluation of the enhancement was difficult due to secondary effects such as a shielding of the inner tubes by the outer ones (antenna effect).

II. EXPERIMENT

Nanotubes were purchased from Nanocarblab and filled with C_{60} fullerenes as reported previously.[28] The diameter distribution of the starting material was determined from Raman analysis and revealed for the peak and for the variance of a Gaussian distribution the values $\bar{D}=1.45$ nm and $\sigma=0.1$ nm, respectively. The resulting mats of bundled peapods were vacuum annealed at 800 K to get rid of any nonencapsulated C_{60}. Measurements of the filling ratio using bulk sensitive electron-energy-loss spectroscopy[29] and Raman spectroscopy[30] revealed a maximum C_{60} occupancy of about 80%. This is very close to the theoretical limit of 95% expected for the tubes used. Under these conditions, the absolute filling of the outer tubes with inner shell tubes which means the ratio of carbon atoms in the outer tubes to the carbon atoms in the peas is 0.28. Of course this ratio remains after the transformation to the DWCNTs. After the 800 K annealing, the peapods were subjected to a high-temperature annealing at 1250 °C and subsequently slowly cooled to room temperature. The resulting DWCNTs exhibited very narrow Raman lines for the RBM down to 0.4 cm^{-1}.[6] Control experiments were performed with slightly smaller tubes grown by laser ablation and purchased from Tubes at Rice. Diameter distribution, again as determined from first and second moments of the RBM response in Raman experiments, was given by $\bar{D}=1.35$ nm, $\sigma=0.1$ nm. Preparation of the DWCNTs was performed as described above. The smaller tube diameter certainly leads to a smaller fraction of DWCNTs relative to the unfilled tubes in these samples as compared to the fraction in the Nanocarblab material but otherwise the results were the same.

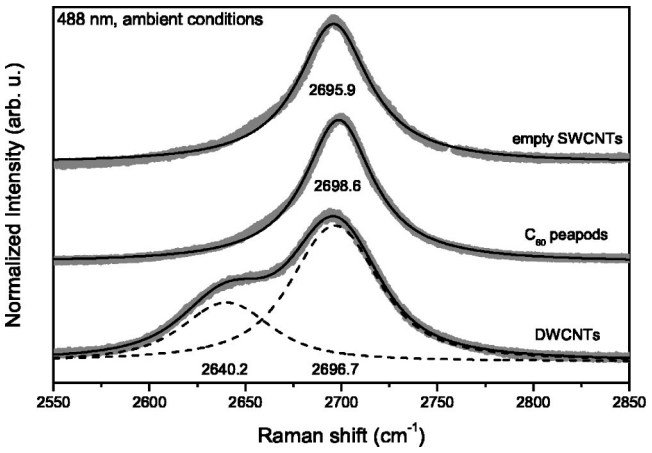

FIG. 3. Raman response of the G′ line in various carbon nanotube materials as exited with a 488 nm laser. Top: pristine nanotubes, center: peapods, bottom: DWCNTs. Dashed lines are Voigtian fits. All spectra are normalized to equal height.

Raman spectra were recorded for laser lines extending from 1.83 to 2.71 eV at ambient conditions using a Dilor xy triple spectrometer with a back thinned and blue enhanced CCD detector. Since the lines of interest here were rather broad, normal resolution was used. The system was calibrated for intensities with Si powder ($\lesssim 250$ μm). The integrated intensity of the Si first-order phonon mode was divided by the incident laser power and then scaled to the Si Raman cross section reported by Renucci *et al.*[31] with a factor f. To obtain the Raman cross section of the G′ mode, its integrated intensity was divided by the incident laser power and then scaled with the same factor f. This procedure corrects for the spectrometer/detector sensitivity and the ω^4 dependence of the Raman process.

III. RESULTS

Figure 3 depicts the response of the G′ mode for the three basic materials under investigation: pristine SWCNTs, peapods, and the resulting DWCNTs, all recorded for the same starting material and the same laser excitation. The response from the pristine material and from the peapods exhibits a smooth line profile with a quasi-Voigtian shape. Looking into details, flat structures and a weak asymmetry can be observed. Such structures could originate from the A_1(L) branch for metallic tubes which is known to be dramatically downshifted due to e-ph coupling.[20] Also, the peak position

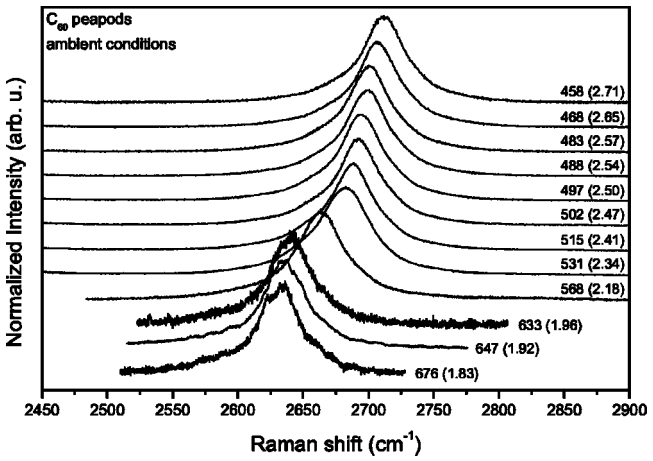

FIG. 4. Raman response of the G′ line in peapods as recorded with various lasers indicated in the figure in nm (eV). All spectra are normalized to equal height.

of the lines is modulated and located at 2696 and 2699 cm^{-1} for the pristine material and the peapods, respectively. The linewidths are about 45 (pristine tubes) and 43 cm^{-1} (peapods). In the case of the DWCNTs, a clear shoulder has developed at the low-frequency side of the G′ response from the outer tubes. This shoulder is assumed to originate from the G′ line of the inner shell tubes. From the Voigtian fits, the line positions for the lower- and higher-frequency peak are at 2640 and 2697 cm^{-1}, respectively, with widths of 55 and 54 cm^{-1}. Since the G′ line is known to exhibit a characteristic resonance profile, it was certainly interesting to check for such profiles in the peapods and in the DWCNTs.

Results for excitation with various lasers are depicted in Fig. 4 for the peapods. The response exhibits the expected result. The G′ line shifts continuously downwards without any dramatic change of its shape. Even though intensities are not yet calibrated, a noticeable drop in the cross section can be expected from the noisy spectra for red laser excitation.

Details of the dispersion and of the resonance excitation can be obtained from a fit of all spectra to Voigtian lines and making use of the calibration of the spectrometer. Results for both the dispersion and the resonance cross section are depicted in Fig. 5. The dispersion exhibits on the average a straight line with a slope of 96.2 cm^{-1}/eV. On top of this line, an oscillatory behavior of the response can be seen, as is well known for the pristine tubes.[23] The slope of the line is slightly smaller than the slope obtained for pristine tubes reported to be 110(3) cm^{-1}/eV.[23]

To obtain the cross section for second-order scattering $|d\chi(\omega)/dQ|^2$, the spectra were calibrated as described above. No additional correction for absorption was included, since it is not well enough known. The cross section obtained in this way is continuously increasing with increasing laser energy with a very broad hump around 2.1 eV, a shoulder around 2.5 eV, and an onset of a peak value at 2.7 eV. Any correction for absorption would only lead to a further increase of the cross section with increasing light energy, since the absorption of bucky paper is continuously increasing with the latter. Thus, the scattering volume is decreasing with increasing energy. The pattern obtained is very similar to the response from the outer shell tubes in the DWCNTs and will therefore be described in more detail in the discussion of the latter results.

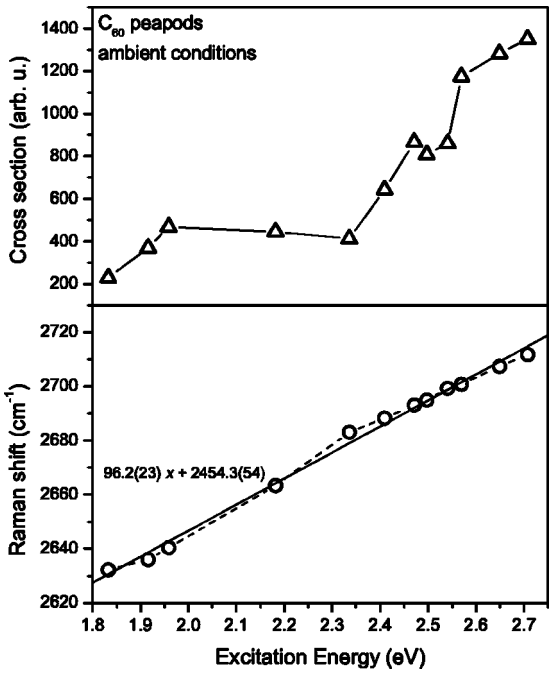

FIG. 5. Dispersion (circles) and Raman cross section (triangles) of the G′ line in peapods. The straight line indicates the linearized response. The dashed line along the experimental points is a guide for the eye and demonstrates the oscillatory behavior.

The response of the G′ lines in the DWCNTs is depicted in Fig. 6 as excited for various lasers. Again clear evidence can be seen for the dispersion effect of both lines and for a resonance behavior which differs for the response from the two concentric shells. In the case of green and yellow laser excitation, the response from the inner tubes is stronger than the response from the outer tubes, even though the concentration of carbons in the inner tubes per volume is only about 28% of the concentration of carbons in the outer tubes. Even-

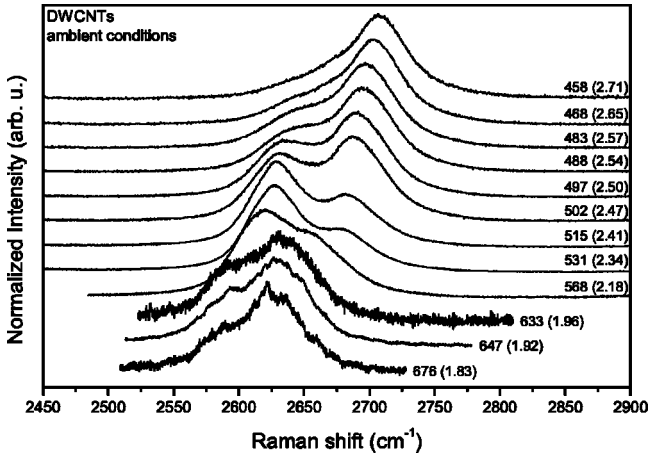

FIG. 6. Raman response of the G′ lines in DWCNTs as recorded with various lasers indicated in the figure in nm (eV). All spectra are normalized to equal height.

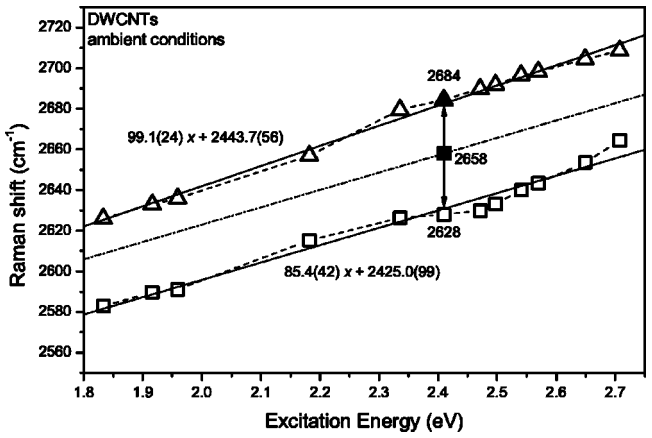

FIG. 7. Dispersion of peak positions for the G′ mode of the outer (upper graph) and inner (lower graph) tubes in a DWCNT system. The dashed lines are guides for the eye to demonstrate the oscillatory behavior. The arrow assigns the distance between outer and inner tube frequency at 2.41 eV. The dash-dotted line is the linearized dispersion expected from individual tube experiments (Ref. 19) if the same slope is assumed as it was observed for the inner shell tubes.

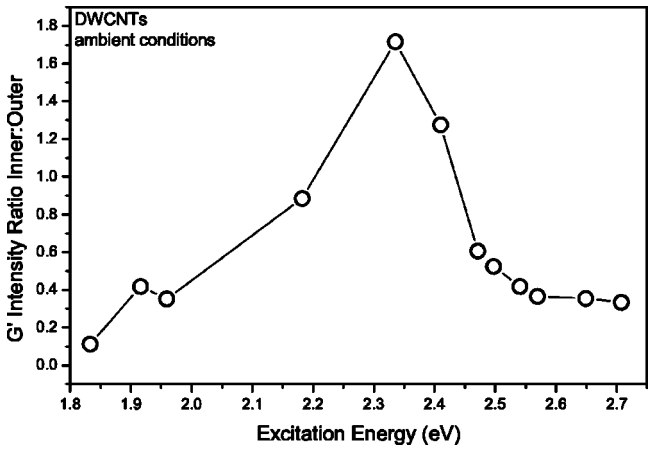

FIG. 8. Peak intensity ratio of inner tube response divided by outer tube response as a function of laser excitation for the G′ modes of DWCNTs.

tually, for excitation with deep red light, the spectra become very weak and the intensity from the inner tubes G′ line drops again to below the response from the outer tubes G′ line. This indicates a rather sharp resonance profile for the inner tubes as compared to the outer tubes.

Like in the case of the peapods, a fit of Voigtian lines to the spectra reveals the dispersion. Figure 7 shows the result for the peak positions as a function of laser energy for both shells. As expected, the relations are quasilinear in both cases with a superimposed oscillation. This oscillation is out of phase for the two shells. In addition, there is a noticeable difference in the slope of the lines. For the outer tubes, we find 99.1 cm^{-1}/eV, whereas the G′ line for the inner tubes yields 85.4 cm^{-1}/eV. This difference is significant as the RMS error as depicted from the figure is much smaller than this difference. In fact, the real error is still considerably lower, since the oscillatory behavior has not been considered in the evaluation of the error.

Figure 7 also depicts the difference in mode frequency for the two G′ lines as evaluated from the straight line to straight line distance at 2.41 eV excitation energy. The obtained distance is much larger than the distance evaluated from the relation

$$\overline{\nu} = 2708.1 - 35.4/D. \quad (1)$$

This relation was derived from a diameter-dependent evaluation of line shifts in individual tube experiments[19] for tubes with diameters between 1.25 and 2.5 nm at 2.41 eV. The above equation yields 2684 cm^{-1} for the outer tube G′ frequency in very good agreement with the result of 2684 cm^{-1} from the DWCNT experiments reported here but much too high values (2658 cm^{-1} as compared to 2628 cm^{-1} observed here) for the inner tubes. The dash-dotted line in the figure indicates the position of the G′ mode for the inner tubes as predicted from Eq. (1) if the same slope is assumed, as was observed for the inner shell tubes.

Evaluation of Raman intensities is not a trivial task and needs a careful calibration and alignment of the experiments. Even then, results may be dressed with a substantial error. If two lines from the same spectrum are compared, these problems are almost excluded and results almost free of error can be expected. The results of Fig. 6 are very suggestive to proceed with the analysis in this form. Peak intensities were obtained from the line fit analysis and the results are shown in Fig. 8. The graph shows a clear maximum at 2.34 eV with an asymmetric energy distribution on the left and on the right side of the peak. No correction for the different amounts of carbon in the two shells was performed since this would only yield a different scale on the ordinate. The peak is expected to be close to the energy where the resonance cross section for the inner tubes has a maximum. At low energies, the response from the inner tubes drops much faster than the response from the outer tubes. In contrast, at high energies the ratio between scattering from inner and outer tubes approaches a constant value.

More detailed information can be drawn from an evaluation of the scattering cross section for the two shells explicitly. Looking at the cross section of the inner tubes in Fig. 9, we recognize immediately the dramatic enhancement as compared to the outer tubes. This enhancement is up to a factor 5 for the corresponding peak positions around 2.3 eV. Also, the resonance is rather narrow and peaks at 2.35 eV as expected from Fig. 8. At the high-energy end of the profile, a second peak appears around 2.65 eV. At the low-energy side, the cross section approaches zero. The overall recorded enhancement of the resonance is about 25. The scattering cross section of the outer tubes is different from the cross section of the inner tubes but very similar to the result obtained for the peapods in Fig. 5. It is continuously increasing with increasing laser energy and exhibits several broad humps or shoulders around 2.15, 2.5, and 2.65 eV. These humps as well as the peak and the shoulder observed for the inner tubes are expected to be correlated to the resonance transitions between the VHSs. The overall enhancement of the cross section for the outer tubes is about 4.

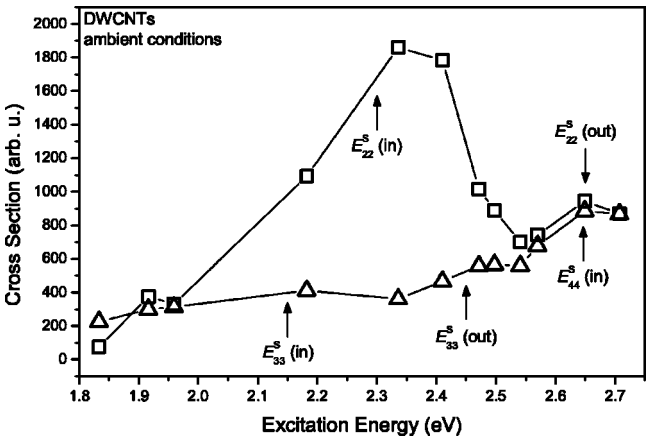

FIG. 9. Raman cross section for the G′ line of the inner (squares) and outer tubes (triangles). The measured response was corrected for the different amounts of carbon in the two shells. Arrows mark the mean transition energies as depicted from Fig. 1.

IV. DISCUSSION

The above findings are interesting on mainly three points: The strongly enhanced e-ph coupling for the inner shell tubes, the resonance profiles for the two concentric shells, and the deviation of the dispersion for the inner tubes from results known so far.

A. Enhanced electron-phonon coupling

Enhancement of e-ph coupling with increasing curvature in carbon cages was already observed from *ab initio* calculations in fullerenes.[32,33] The increasing contribution of the σ bonding to the interaction between the carbon atoms is the reason. Results in the same direction were obtained for the nanotubes. Even though such results were evaluated for the e-ph coupling in the conduction band[27] or exhibit a strong dependence on chirality,[34,35] they can be expected to provide qualitative information on the relation between coupling and tube diameter. From an extrapolation of the e-ph coupling constants evaluated in Ref. 27, the latter are about 1.6 times higher for the tubes with diameter 0.7 nm as compared to the tubes with 1.45 nm. Since the e-ph coupling enters to the fourth power into the Raman intensity for a two-phonon process, intensities from the inner shell tubes can be expected to be eight times higher as compared to the intensities from the outer shell tubes. The enhancement of the cross section observed experimentally is not quite as high. This may be due to a partial shielding of the inner tubes by the outer tubes or by field-induced charges which generate a depolarization field[36] (antenna effect). A first experimental evidence for the enhanced e-ph coupling was already obtained from the strongly enhanced Raman response reported for the RBM modes.[6] The experimental demonstration of the enhancement of the e-ph coupling is important for the characterization of the inner shell nanotubes. Since these tubes are highly defect-free, any response from the D line should be very weak unless enhanced e-ph coupling raises the scattering cross section.

B. Resonance profiles for the two concentric shells

The resonance profile for Raman excitation in SWCNTs is determined by transitions between VHSs as they are plotted in Fig. 1. Since Fig. 1 is based on dispersed HiPco tubes wrapped with SDS, it is not straightforward to apply it to DWCNTs. In fact, Fantini *et al.*[15] reported that the transition energies of HiPco tubes in bundles are about 75 meV below the corresponding energies of the SDS wrapped tubes. Fortunately, the resonances we are discussing for the G′ lines are rather broad. This means the results of Fig. 1 still provide valuable information for the interpretation of the data. This holds in particular since curvature effects, which are relevant for the small diameter inner tubes, are included in the calculation. Also, it must be kept in mind that the cross sections we are discussing here refer to the overall material consisting of many different tubes. It is not the cross section of a single nanotube itself. For the assignment of the observed resonances, ingoing as well as outgoing light must be considered, since for the high frequencies under consideration the difference in transition energy can be as high as 0.33 eV.

Starting with the analysis of the inner shell tubes and comparing the resonance positions with the data of Fig. 1, we can assign the resonance at 2.3 eV to the transitions E_{22}^S. In addition, ingoing resonances for E_{11}^M transitions contribute. According to Fig. 1, the resonance can be rather broad, up to 1 eV, which is indeed the case. Thus, according to the condition of the experiment, the resonance is determined by the distribution of tube diameters rather than by the widths of the transitions between VHSs. The resonance at 2.65 eV fits to the transition E_{22}^S for the outgoing photons. In this case, the excitation energy has to be about 0.33 eV higher than the resonance transition. This is exactly the case for the shoulder in the cross section. The overall background in the cross section comes from the conventional double resonance and from the less efficient triple resonance which does not involve two VHSs.

For the outer tubes, we can correlate the broad low-energy hump around 2.15 eV with the resonance at the E_{33}^S transition for the incoming photons. The shoulder at 2.5 eV fits well to the E_{33}^S transition for the outgoing photons, whereas the structure at highest energy (2.65 eV) matches well with the ingoing E_{44}^S transition. The broadening and smearing out of the resonances is not surprising. Particularly for the outer tubes, it originates not only from conventional double resonances but also from the increasing influence of the chiral angle on the transition energies with increasing folding index, as can be seen from Fig. 1.

C. Dispersion of the G′ line for the high curvature inner tubes

The difference in the G′ line dispersion between inner shell and outer shell tubes is of particular interest. This difference refers to the slope of the dispersion as well as to the absolute line positions. Since the former is a replica of the phonon dispersion around the *K* point, a flattening of this dispersion with increasing curvature must be concluded from the smaller value of the inner tubes dispersion.

Concerning the absolute value of the downshift observed for the inner tubes G′ lines as compared to the outer shell

positions, we must keep in mind that Eq. (1) was derived from single tube experiments with diameters between 1.25 and 2.5 nm. The leading constant of 2708 cm^{-1} is the frequency for the G′ mode in graphite. As the experiments in Ref. 19 demonstrate, curvature decreases all high-frequency optical modes. This is consistent with *ab initio* calculations for the G mode as a function of diameter[20] where a dramatic and nonlinear decrease of the mode frequency was found for tubes with diameters <1 nm. Thus, the discrepancy between the results from the linearized decrease given by Eq. (1) and from the inner shell tubes is understandable from the small tube diameter. The influence of high curvature has been reported also for the RBMs, but due to the low frequency of the latter it is only a few wave numbers and difficult to observe.[25] In the case of the G′ mode, the relative deviation from linearity is about the same, but due to the high frequency it comes out between 20 and 30 cm^{-1} (depending on the exciting laser used) and is therefore easily detectable. Calculation of the downshift is unfortunately difficult since the *K* point phonons of all branches and of all tubes contribute.

Because of the folding of the graphite Brillouin zone into the nanotube zone and because of the nanotube curvature, the G band in nanotubes contains several modes with different symmetries. The tangential modes that are Raman active exhibit *A*, E_1, and E_2 (A_{1g}, E_{1g}, and E_{2g} for symmorphic groups) symmetries.[37] Assuming that the whole optical branch is modulated by curvature in the same way, we can scale the *K* point frequencies to the Γ point modes for large tube diameters and thus reveal a mapping of the former on the tube diameters. The mapping was performed in two ways. In the first attempt, only the transversal E_2 modes were considered as the main contributors to the G′ line. In a second attempt, the average frequency at the Γ point of all branches was considered and used to map the position of the G′ line as a function of tube diameter. The mapping was done such that the calculated E_2(T) frequency at $D = 1.5$ nm was scaled to the experimental G′ position of the outer tubes for 2.41 eV excitation. The averaged values were scaled the same way.

The diameter dependences of the Raman frequencies in Fig. 10 were fitted with $\overline{\nu} = A + B/D$. For the E_2(T) and averaged G mode branches, we get $\overline{\nu_G} = 1662(6) - 62(6)/D$ and $\overline{\nu_G} = 1626(7) - 53(6)/D$, respectively. For the scaled G′ frequencies, we get $\overline{\nu_{G'}} = 2766(9) - 103(9)/D$ and $\overline{\nu_{G'}} = 2753(11) - 90(11)/D$. A mapping for the other excitation energies gave similar results.

The good agreement between observed (asterisks) and calculated (open symbols) results justifies the interpretation of the discrepancy between single tube experiments and the results reported here as due to curvature effects as well as the down mapping procedure. Interestingly, a simple diameter scaling in Eq. (1) with diameters as calculated from *ab initio* DFT (Ref. 25) does not give the correct behavior. In contrast, since DFT yields higher tube diameters as compared to the tight-binding values, the G′ line frequencies would upshift toward the line from the outer tubes as compared to the results from Ref. 19.

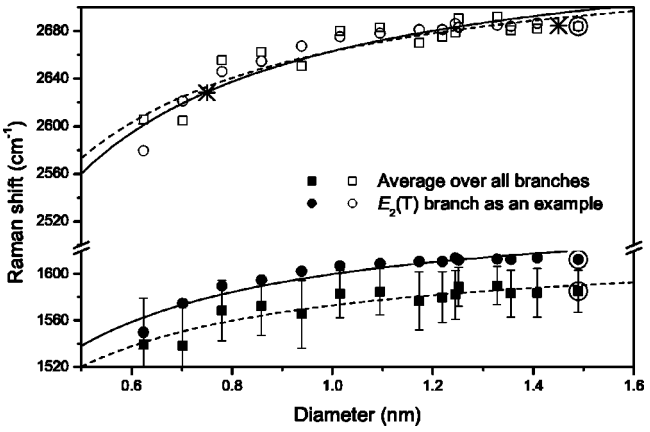

FIG. 10. Comparison of calculated and observed G′ line frequencies. Bullets and full squares are G line frequencies as calculated from Dubay *et al.* (Ref. 20) for the $E_2(T)$ branch and as averaged for all branches (the error bars depict the standard deviation). The circled points were used for the scaling. The open symbols are the scaled frequencies for the G′ line. The two asterisks represent the experimental results for the outer and inner tubes at 2.41 eV. The lines are fits as described in the text.

V. SUMMARY

In summary, we have reported detailed experimental results for the Raman line position and intensity for the G′ line in DWCNTs. The response appears as a double-peaked band with a characteristically different resonance cross-section profile. Both components of the band exhibit the expected dispersion but the value of the inner shell tubes is lower (85.4 cm^{-1}) as compared to the value of the outer shell tubes (99.1 cm^{-1}). The superimposed oscillatory behavior has opposite phase for the two tube systems. The downshift in frequency between the G′ line from the inner tubes and from the outer tubes is significantly larger than expected from measurement on conventional diameter tubes. This is demonstrated to be a consequence of the strong curvature of the inner shell tubes. Finally, the scattering cross section reveals the nature of the triple resonance from the VHSs.

Note added in proof. Recently, a spectrochemical analysis of DWCNTs was reported, where the spectroscopic behavior of the G′ line in pristine and doped DWCNTs is discussed.[38]

ACKNOWLEDGMENTS

Work was supported by the FWF in Austria (P 14893) and by the EU projects NANOTEMP (BIN2-2001-00580) and PATONN (MEIF-CT-2003-501099). E.O. acknowledges funding from the RAS program "Low-dimensional quantum structures." Valuable discussions with J. Kürti, V. Zólyomi, and G. Kresse are gratefully acknowledged. We thank V.N. Popov for supplying his calculated transition energies.

[1] R. Saito, G. Dresselhaus, and M. S. Dresselhaus, *Physical Properties of Carbon Nanotubes* (Imperial College Press, London, 1998).
[2] M. S. Dresselhaus, G. Dresselhaus, and P. Avouris, *Carbon Nanotubes: Synthesis, Structure, Properties, and Applications* (Springer, Berlin, 2001).
[3] S. Reich, C. Thomsen, and J. Maultzsch, *Carbon Nanotubes* (Wiley-VCH, Weinheim, 2004).
[4] B. W. Smith, M. Monthioux, and D. E. Luzzi, Nature (London) **396**, 323 (1998).
[5] S. Bandow, M. Takizawa, K. Hirahara, M. Yudasaka, and S. Iijima, Chem. Phys. Lett. **337**, 48 (2001).
[6] R. Pfeiffer, H. Kuzmany, C. Kramberger, C. Schaman, T. Pichler, H. Kataura, Y. Achiba, J. Kürti, and V. Zólyomi, Phys. Rev. Lett. **90**, 225501 (2003).
[7] Z. K. Tang, H. D. Sun, J. Wang, J. Chen, and G. Li, Appl. Phys. Lett. **73**, 2287 (1998).
[8] Z. K. Tang, L. Zhang, N. Wang, X. X. Zhang, G. H. Wen, G. D. Li, J. N. Wang, C. T. Chan, and P. Sheng, Science **292**, 2462 (2001).
[9] F. Simon, A. Kukovecz, C. Kramberger, R. Pfeiffer, F. Hasi, H. Kuzmany, and H. Kataura, Phys. Rev. B (to be published).
[10] R. Saito, G. Dresselhaus, and M. S. Dresselhaus, Phys. Rev. B **61**, 2981 (2000).
[11] V. N. Popov, New J. Phys. **6**, 17 (2004).
[12] C. L. Kane and E. J. Mele, Phys. Rev. Lett. **93**, 197402 (2004).
[13] J. Kürti, V. Zólyomi, M. Kertesz, and S. Guangyu, New J. Phys. **5**, 125 (2003).
[14] H. Kataura, Y. Kumazawa, Y. Maniwa, I. Umezu, S. Suzuki, Y. Ohtsuka, and Y. Achiba, Synth. Met. **103**, 2555 (1999).
[15] C. Fantini, A. Jorio, M. Souza, M. S. Strano, M. S. Dresselhaus, and M. A. Pimenta, Phys. Rev. Lett. **93**, 147406 (2004).
[16] R. B. Weisman and S. M. Bachilo, Nano Lett. **3**, 1235 (2003).
[17] R. A. Jishi, L. Venkataraman, M. S. Dresselhaus, and G. Dresselhaus, Chem. Phys. Lett. **209**, 77 (1993).
[18] J. Kürti, G. Kresse, and H. Kuzmany, Phys. Rev. B **58**, R8869 (1998).
[19] A. G. Souza Filho, A. Jorio, G. G. Samsonidze, G. Dresselhaus, M. A. Pimenta, M. S. Dresselhaus, A. K. Swan, M. S. Ünlü, B. B. Goldberg, and R. Saito, Phys. Rev. B **67**, 035427 (2003).
[20] O. Dubay, G. Kresse, and H. Kuzmany, Phys. Rev. Lett. **88**, 235506 (2002).
[21] C. Thomsen and S. Reich, Phys. Rev. Lett. **85**, 5214 (2000).
[22] J. Maultzsch, S. Reich, and C. Thomsen, Phys. Rev. B **64**, 121407(R) (2001).
[23] J. Kürti, V. Zólyomi, A. Grüneis, and H. Kuzmany, Phys. Rev. B **65**, 165433 (2002).
[24] V. Zólyomi, J. Kürti, A. Grüneis, and H. Kuzmany, Phys. Rev. Lett. **90**, 157401 (2003).
[25] C. Kramberger, R. Pfeiffer, H. Kuzmany, V. Zólyomi, and J. Kürti, Phys. Rev. B **68**, 235404 (2003).
[26] S. Bandow, G. Chen, G. U. Sumanasekera, R. Gupta, M. Yudasaka, S. Iijima, and P. C. Eklund, Phys. Rev. B **66**, 075416 (2002).
[27] L. X. Benedict, V. H. Crespi, S. G. Louie, and M. L. Cohen, Phys. Rev. B **52**, 14 935 (1995).
[28] H. Kataura, Y. Maniwa, T. Kodama, K. Kikuchi, K. Hirahara, K. Suenaga, S. Iijima, S. Suzuki, Y. Achiba, and W. Krätschmer, Synth. Met. **121**, 1195 (2001).
[29] X. Liu, T. Pichler, M. Knupfer, M. S. Golden, J. Fink, H. Kataura, Y. Achiba, K. Hirahara, and S. Iijima, Phys. Rev. B **65**, 045419 (2002).
[30] H. Kuzmany *et al.*, Appl. Phys. A: Mater. Sci. Process. **76**, 449 (2003).
[31] J. B. Renucci, R. N. Tyte, and M. Cardona, Phys. Rev. B **11**, 3885 (1975).
[32] O. Gunnarsson, Rev. Mod. Phys. **69**, 575 (1997).
[33] M. Schluter, M. Lannoo, M. Needels, G. A. Baraff, and D. Tománek, Phys. Rev. Lett. **68**, 526 (1992).
[34] M. Machón, S. Reich, J. M. Pruneda, C. Thomsen, and P. Ordejón, in *Proceedings of the XVII IWEPNM* (AIP, NY, 2003), pp. 427–430.
[35] M. Machón, S. Reich, J. Maultzsch, P. Ordejón, and C. Thomsen, in *Proceedings of the XVIII IWEPNM* (AIP, NY, 2004), pp. 381–384.
[36] L. X. Benedict, S. G. Louie, and M. L. Cohen, Phys. Rev. B **52**, 8541 (1995).
[37] A. Jorio, G. Dresselhaus, M. S. Dresselhaus, M. Souza, M. S. S. Dantas, M. A. Pimenta, A. M. Rao, R. Saito, C. Liu, and H. M. Cheng, Phys. Rev. Lett. **85**, 2617 (2000).
[38] M. Kalbáč, L. Kavan, M. Zukalová, and L. Dunsch, Carbon **42**, 2915 (2004).